



# Operational Failure of Vertical Roller Attached to a Grinding Mill: Root Cause Analysis

M. Ghosh · B. Mahato · B. Ravi Kumar

Submitted: 3 October 2023 / Accepted: 20 October 2023 / Published online: 21 November 2023  
© ASM International 2023

**Abstract** In the present incident, one of the rollers of grinding mill in cement plant failed during operation, exhibiting longitudinal cracking over inner surface. Deposition welding was carried out just before the incident to match the worn-out profile of the roller. Investigation revealed that the subsurface of the cracked region contained discontinuities like blow holes ( $\leq 1.0$  mm) and fine cracks (0.2–2.0 mm length). Chemical analysis of the alloy showed low nickel (0.5 wt.%) and high tungsten ( $\sim 1.0$  wt.%) concentration. The deviation in composition reduced the ductility of the component. Microstructure of the alloy consisted of complex carbides (50–200  $\mu\text{m}$ ) embedded in martensite–austenite matrix. Under cyclic loading, the fatigue crack was initiated from subsurface containing discontinuities and bulky carbides. Low toughness ( $\sim 2$  J) and high residual tensile stress ( $\sim 170$  Mpa) of the material facilitated crack propagation through thickness direction. Final failure of the component occurred due to overload.

**Keywords** Casting · Cast iron · Fatigue · Fractography · Metallography

## Introduction and Background Information

Grinding is one of the major operations in heavy engineering industries involving in mineral beneficiation of ores, mining of coal, production of pig iron, and manufacturing of cement. Normally crushing and grinding of

raw materials are carried out in autogenous mill, ball mill, pebble mill, rod mill, and roller mill. The selection of mill depends on nature of feed material and required quality of final product.

Several reasons have been described in studies for the failure of vertical roller in grinding mill. Unnatural vibration, short comings in maintenance, deviation in operating parameters and inferior grade of raw materials play a significant role in such failures [1]. Failure of the disk attrition mill used for grinding quartz particles has been reported in recent past. The mill consisted of a gigantic gray cast iron frame, gravity feeder port, runner, and heavy-duty motor. In-depth investigation of the failed disk revealed severe wear of grinding plates. It was concluded that primary feed material was harder than grinding plate material, which resulted in wear and subsequent failure of components [2]. Neves and his co-workers have reported the failure of the ball mill trunnion during service [3]. It was found that during operation lubrication was in-sufficient. Severe friction raised thermal stress, and the crack was initiated. Statistical analysis considering de-generation of component and subsequent failure of jaw crushing unit of a mineral beneficiation plant was investigated by Sinha et al. [4]. The increasing wear rate of the crusher with time was attributed to the wide variation in the quality of raw materials. In this perspective, premature failure of a semi-autogenous grinding mill has been also discussed. The equipment was used in iron ore dressing. The alloy was hypereutectoid low-alloy chromium steel. The shell liner wall of the grinding unit was severely damaged. The material failure of shell wall was ascribed to the presence of coarse pearlite and cementite network instead of the preferred microstructure of tempered martensite with a small amount of retained austenite [5].

---

M. Ghosh (✉) · B. Mahato · B. R. Kumar  
Materials Engineering Division, CSIR-National Metallurgical  
Laboratory, Jamshedpur, India  
e-mail: mainakg@nmlindia.org

In present incident, failure took place in a particular grinding mill of a cement plant. The grinding mill was used to produce extremely fine powder in wet condition from clinker. Grinding of feed materials occurred between multiple sets of spring assembled vertical rollers and table liners. During operation, the grinding mill experienced extreme crushing load. Therefore, satisfactory strength with adequate toughness was desirable for vertical roller material to withstand against severe wear and abrasion. However, wear of vertical roller and table liner became unavoidable. To compensate material loss and match the profile of worn-out roller surface and table liner, deposition welding has been carried out for the vertical roller as per recommendation of OEM. After third time deposition welding, consecutively two rollers failed within a few weeks.

The failure of vertical roller was immediately followed by visual examination and exhibited longitudinal cracking through the inner wall of the component. The plant never experienced such kind of catastrophe for the last ten years; thus, it became necessary to explore the origin, nature, and specific reason of component failure to prevent recurrence of such incident.

## Experimental Procedure

### Case study

The schematic of grinding mill and isolated vertical roller assembly is shown in Fig. 1. During operation of grinding mill, normal load was maintained below  $\sim 70$  bar depending on the characteristics of feed material. The grinding mill consisted of a table with

diameter  $\sim 2500$  mm and grinding track of  $\sim 1600$  mm diameter. The mill could accommodate a feed size of  $< 2000 \mu\text{m}$ . As per OEM recommendation, maximum number of allowable deposition welding to restore worn-out surface profile depended on original thickness of material. The welding method was metal active gas welding (MAG) using an iron base high Cr filler rod. Post-weld heat treatment has been avoided after deposition welding.

After installation, two times salvaging welding have been carried out during a span of  $\sim 15,000$  h of service for the damaged roller. Before every deposition welding, after re-dressing the worn-out surface, where the component exhibited mismatch with respect to normal profile, dye penetration test has been done to ensure absence of discontinuities in any form to the freshly exposed surface. After deposition welding, once again visual examination and dye penetration test were performed. The examination did not reveal any crack/heterogeneity. These examinations have been carried out at user end, and as an obvious requirement for the investigation, the information was shared.

Expected life span of vertical roller was  $\sim 1.0$  L h of service with intermittent welding as per requirement. For this vertical roller, after third time deposition welding, the component was once again put into operation. Finally, the component failed after completing  $\sim 21,500$  h of total service life, which was nearly one-fourth of the predicted life.

### Methodology

Based on the background information available from the end user, it was planned to carry out the investigation in steps. The methodology included visual examination,

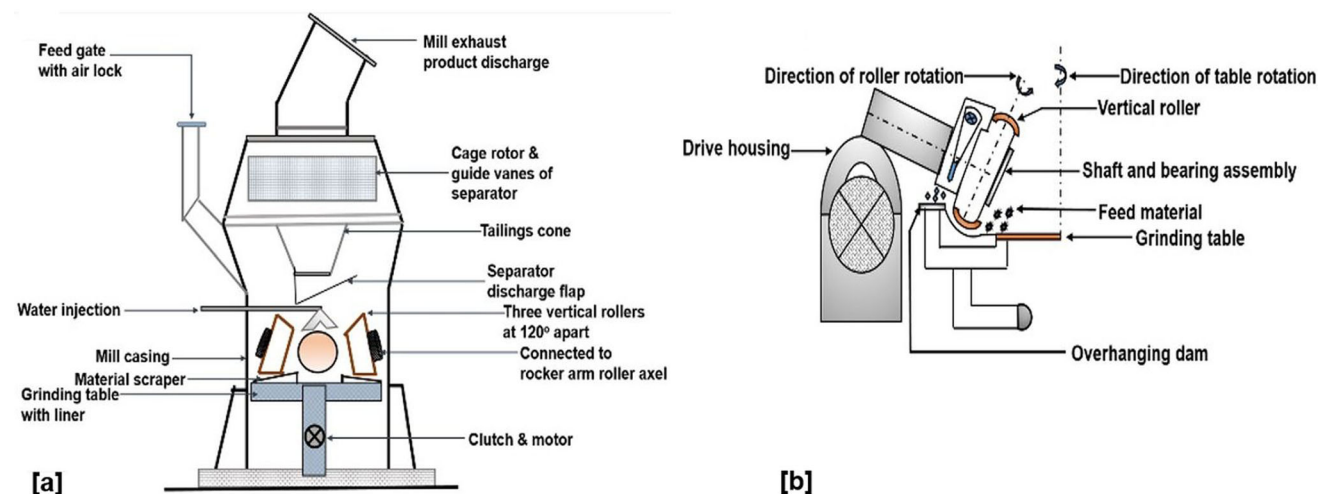


**Fig. 1** Schematic diagram of grinding mill in cement plant (a) position of vertical rollers, where the central one failed in present incident, and (b) isolated vertical roller assembly (Not to scale)

determination of chemical composition, microstructural examination, macro-hardness measurement, fractography of failed surface, and residual stress analysis. In subsequent sections, technique/methodology of each activity has been discussed.

### Visual Observation

The schematic of grinding mill along with the position of three rollers is given in Fig. 1a. An isolated assembly of a vertical roller has been also presented (Fig. 1b). As depicted in Fig. 1a, the central roller was failed during service. The defective component was removed from the assembly for investigation. The examination of the failed region has been carried out by low power magnifier (10X) to explore general feature and identify sampling locations (Fig. 2).

### Chemical Composition Analysis

The chemical composition of the component and weld filler alloy has been determined. Sampling for bulk analysis was carried out from the inner surface of the damaged component. Exact location of sampling was  $\sim 3.0$  cm away from the cracked region. The concentration of major chemical species was estimated using Inductively Coupled Plasma-Optical Emission spectroscopy (ICP-OES, Thermo-Fischer). Quantity of non-metallic elements like carbon, sulfur, and phosphorous was done using LECO gas analyzer. The chemical analysis of the failed component was compared with standard specification.

### Evolution of Microstructure

Sampling has been done close to the cracked surface of the component (Fig. 2a). Initially, a segment containing the failed location was cut from damaged component by abrasive wheel under proper cooling. Further sectioning was performed using EDM to obtain samples for microscopy. The surface of sample coupons was parallel to fracture plane. The specimens were polished by conventional metallographic technique, etched with 3% Nital after proper cleaning and examined in an optical microscope (Leica DM300) at different magnifications.

### Hardness Measurement

Bulk hardness of the component was evaluated over the subsurface just below the fracture plane. Sampling has been done by the same procedure, by which specimens for optical microscopy were obtained. The hardness was evaluated in Brinell scale (Cmetco DM 3000) using 3000 N load, 10-mm-diameter tungsten carbide ball, and 30 s dwelling time. Result was compared with the standard specification of similar alloy to assess the deviation in hardness at the close vicinity of crack formation.

### Fractography

Sampling has been done carefully from multiple locations considering the failed location (Fig. 2b–c). Over the bulk specimen after first phase sampling, vulnerable locations have been identified (circles of Fig. 2c). Specimens were further obtained from the locations by slow-speed diamond

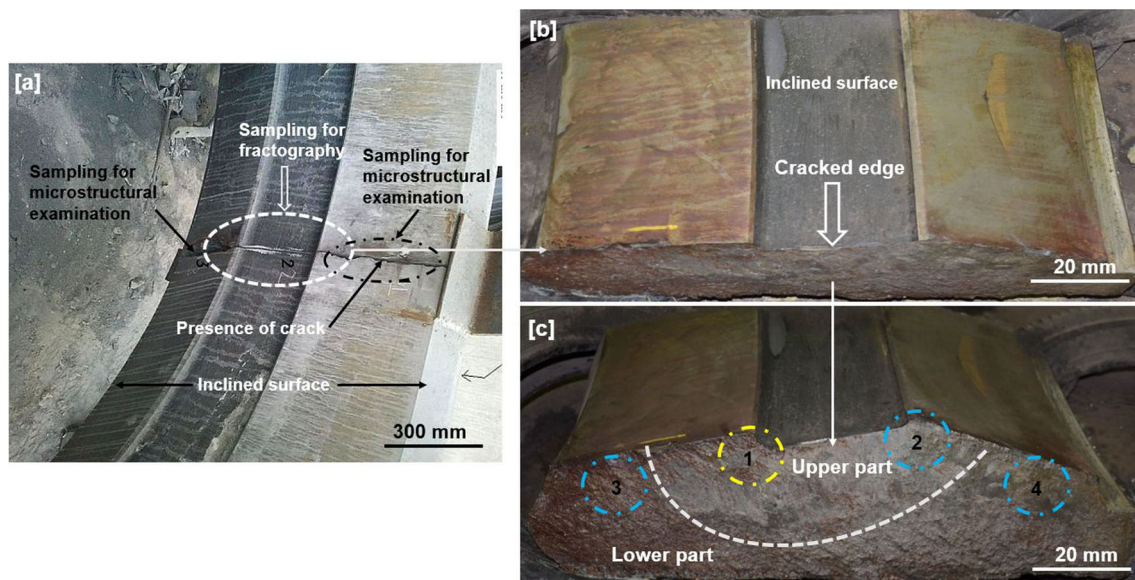


**Fig. 2** Macro-image of damaged component after removing shaft and bearing assembly (a) cracking over the inner surface of roller, (b) bulk sampling from damaged component, and (c) enlarged view of the fracture surface (Color figure online)

cutter (Buehler IsoMet). All these samples were thoroughly cleaned by sonication and observed in a scanning electron microscope (JEOL JSM 840A) at 15 kV operating voltage. Samples 1 and 2 corresponded to identical locations, and both were examined. Significant features were present in Sample 1, and the fractography was discussed in detail for the same in subsequent section. Samples 3 and 4 were practically featureless and thus not reported in present manuscript.

#### *Determination of Impact Toughness*

Sampling has been done along the longitudinal axis of the component parallel to crack propagation and prepared according to ASTM E23-2016 for impact test (MTS). The notch was pointed toward inner surface of the roller. The test has been carried out at room temperature to reveal the effect of structural constituents on impact toughness.

#### *Evaluation of Residual Stress*

Deposition welding without any post-weld heat treatment has been performed over vertical roller surface as mentioned earlier; therefore, it was decided to estimate residual stress over the subsurface of fracture plane of the component. Portable x-ray stress measurement unit (XTress 3000) was used, and  $\text{Sin}^2 \psi$  methodology was adopted during the experiment. Other parameters during investigation were Cr  $K\alpha$  radiation, 30 kV potential, 5 mA current density, and 3 mm collimator diameter. The technique did not require any stress free similar/identical specimen. Both peak shift and broadening were considered in characteristic x-ray spectrum to estimate the nature and value of residual stress at the location of interest.

## **Results**

The major observations of all experiments have been described in the following sections.

#### *Visual Examination*

Cracking was observed along the longitudinal direction over the inner surface of the broken vertical roller. The crack was nearly straight without any branching (Fig. 2a). Sampling from failed location revealed two different morphologies over fracture surface (Fig. 2c). The upper part, which was close to open end of inner periphery, contained a ‘kidney-shaped’ region (dimension  $\sim 8$  cm major axis  $\times \sim 4$  cm minor axis, encircled by dotted line). Rest of the part (lower region, outside of dotted region) exhibited rough irregular surface. ‘kidney’-shaped

region was bright and smooth with respect to rest of the area. The feature over fracture plane manifested fatigue crack propagation, followed by fast fracture as demonstrated by the ‘dull and rough’ appearance of rest of the fracture surface [6].

Subsurface region of the inner wall of the vertical roller adjacent to the main crack was examined. The material contained nearly spherical-shaped discontinuities of various diameters and at diverse depth levels from the surface (Fig. 3c–d). The presence of blow/pin holes and pores with dimension 0.2–1.0 mm might be considered as casting defect. Isolated and inter-connected micro-cracks through these discontinuities were also found with multiple branching (Fig. 3a–c).

#### *Composition Analysis*

Bulk composition of the vertical roller and the filler alloy used for deposition welding is collated in Table 1. The specification of roller material was ASTM A532 Class I Type D as per available data. With respect to the standard specification, nickel content was extremely low in the investigated alloy.

The filler alloy composition was nearly at par with bulk analysis except for Cr and Mo content. Chromium and molybdenum concentration was significantly high in filler alloy. The specification did not show any tungsten content; however, the same element was present within the component as well as in the filler alloy.

#### *Microstructural Investigation*

Optical microstructure of the alloy is shown in Fig. 4. Both the specimens exhibited nearly the same feature; hence, the images of one specimen have been furnished here (Fig. 2a). The component represented a particular class of white cast iron. The microstructure consisted of primary dendrite and carbide eutectic (Fig. 4a). Shaded matrix was predominantly martensitic in nature with small amount of austenite (Fig. 4b). The eutectic was a mixture of rod/blade-shaped bright complex carbides (M7C3) embedded within the matrix (Fig. 4c–d). From geometry, two types of carbides were found: One of them was inter-connected, and the other was isolated (Fig. 4b). Isolated carbides were small ( $< 50$   $\mu\text{m}$  length and  $< 10$   $\mu\text{m}$  width). Large size island/inter-connected/irregular-shaped carbides were also present in substantial quantity ( $> 50$   $\mu\text{m}$ ) (Fig. 4c).

#### *Fractography*

All four specimens as mentioned in “[Fractography](#)” section were initially examined in SEM for revealing general features of fracture surface. Sample 1 of Fig. 2c exhibited

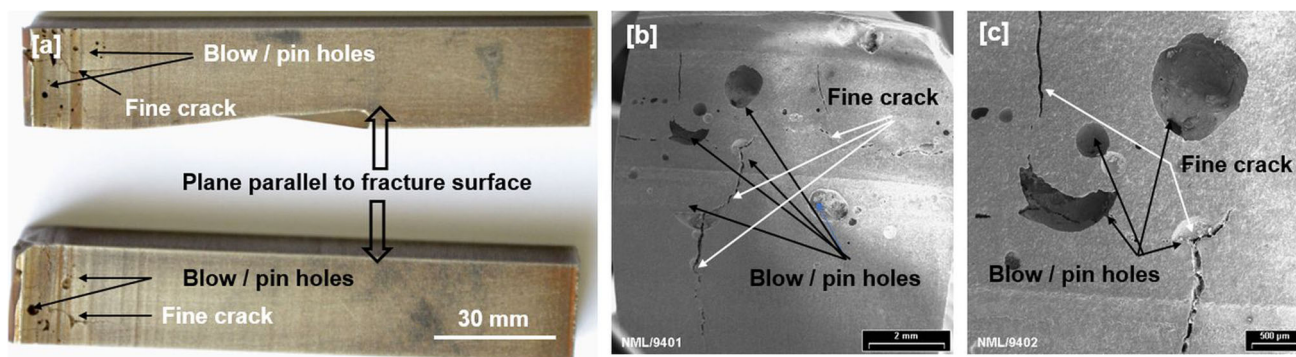
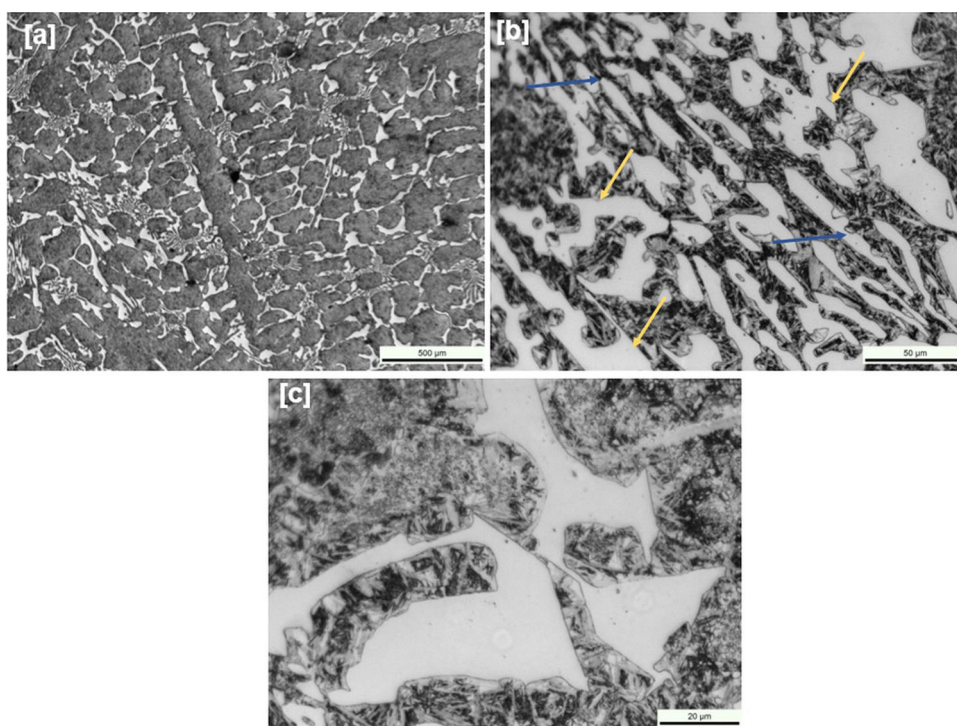


**Fig. 3** Image of subsurface of cracked region (a) distribution of blow/pin holes over the subsurface of fracture plane, (b) and (c) enlarged view of Fig. 3a for two different locations

**Table 1** Chemical composition of component material and filler alloy

Alloy	Elements in wt.%									
	C	Si	Mn	Cr	Ni	Mo	S	P	W	Fe
ASTM A532 class I type 'D'	2.5–3.6	2.0 max.	2.0 max.	7–11	4.5–7.0	1.5 max.	0.15 max.	0.1 max.	...	Bal.
Bulk composition	3.0	1.8	0.90	10.0	0.54	0.60	0.01	0.03	1.0	Bal.
Filler composition	...	...	...	18.0	0.27	3.62	...	...	1.4	Bal.

**Fig. 4** Optical micrographs of component near damaged location (a) overall solidification structure, (b) large inter-connected (white arrow) and isolated small size carbide distribution (yellow arrow) within matrix, and (c) bright irregular-shaped chunky carbide (Color figure online)



marked difference with respect to others and was further investigated in detail (Fig. 5). Figure 5a presents low magnification image of the location as shown in Fig. 2c. Overall appearance represented the characteristic of transgranular cleavage fracture with limited ductility. The crack initiation location contained large size carbides and

discontinuities (Fig. 5b). Characteristic x-ray spectrum was obtained from the location shown in Fig. 5b (cross-point) and endorsed the presence of complex carbides (Fig. 5f). Under cyclic loading, when the crack propagated, striations were formed over fracture surface and became the signature of fatigue (Fig. 5c). The investigated alloy

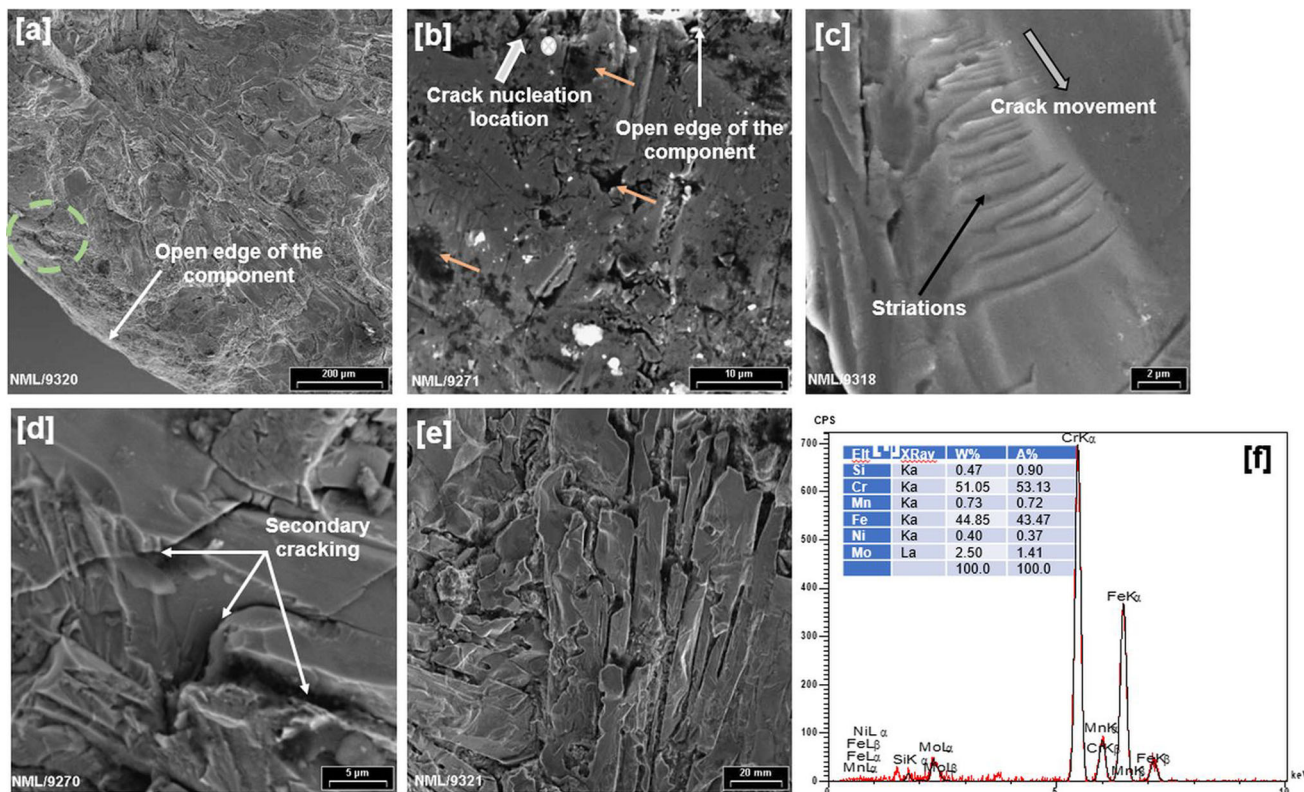


**Fig. 5** Fractographs of location marked in Fig. 2c (yellow circle) (a) overall image exhibiting location of fatigue crack initiation (green circle) (b) magnified image of marked region of Fig. 5a showing fracture initiation location, surrounded by chunky second phase and pin holes (small arrows) (c) local striations and crack propagation, (d) secondary cracking in the adjacent region of crack propagation, (e)

fragmentation of complex carbides, and (f) characteristic x-ray spectrum and semi-qualitative analysis of cross-marked region of Fig. 5 (Color figure online)

**Table 2** Bulk hardness of the component

Component	Brinell scale
Broken roller tire hub	~ 654 ± 6
Specified data	550–600

was brittle in nature. Therefore, state-of-the-art beach marks over a wide zone has not been found during fractographic examination [7, 8]. Secondary cracking/decohesion between precipitate and matrix was evident over fracture surface owing to limited ductility of the alloy and heavy grinding load (Fig. 5d). The complex carbides adjacent to the area of crack propagation were also fragmented endorsing the limited capability of the alloy to accommodate deformation under severe stress.

**Hardness Evaluation**

The bulk hardness of the component is furnished in Table 2. From the specification of the alloy, the bulk

hardness of the same for the sand cast component has been also given.

With respect to the specification, the broken vertical roller exhibited relatively higher hardness.

**Impact Testing and Corresponding Fracture Surface Investigation**

The impact toughness of the alloy at room temperature was 2 ± 0.5 J. The specimen for impact testing was chosen in such a fashion that the defects like micro-crack/blow holes/pores were absent for the prepared specimen. Standard data for the impact toughness of this alloy were not available and hence cannot be compared; however, the result appeared extremely low indicating limited ductility of the alloy.

Inter-granular faceted morphology has been observed in fractographs of the impact tested specimens (Fig. 6). The overall appearance of fracture surface of the samples envisaged negligible ductility of the alloy.

**Fig. 6** Fractographs of impact tested specimens (a) intergranular failure and (b) faceted fracture surface

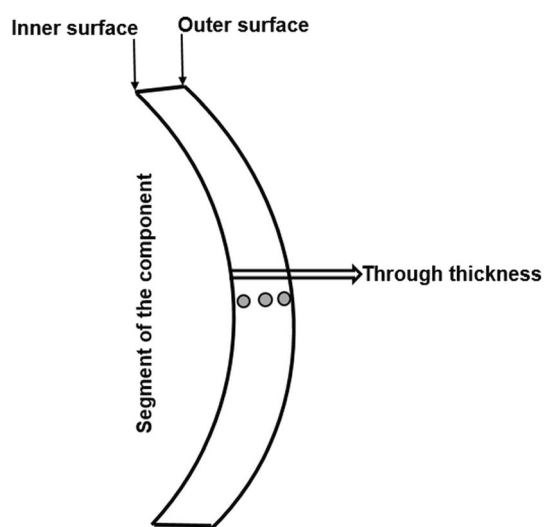
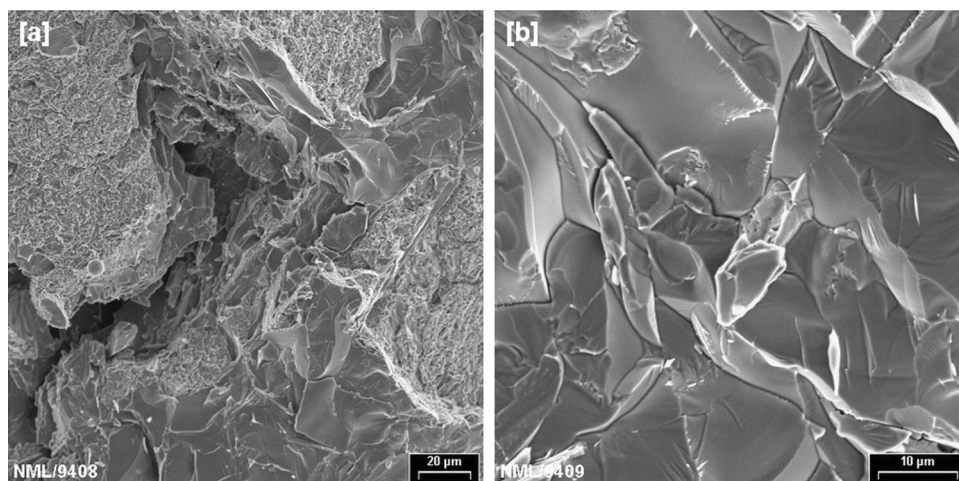


**Fig. 7** Direction of residual stress measurement (arrow mark with schematic locations)

### Residual stress analysis

Surface residual stress (RS) has been measured for the damaged component. The measurement was done just below the fracture surface and its surrounding exhibiting very high tensile residual stress of the order of  $\sim 170$  MPa (Fig. 6). Such high tensile residual stress perpendicular to the plane of crack propagation further contributed to fast movement of the crack (Fig. 7).

### Discussion

Visual examination revealed that subsurface of fractured component contained discontinuities of various dimensions and fine inter-connecting cracks. The discontinuities were perhaps the resultant of excessive super-heat and high

quantity of dissolved gases within melt before casting. High amount of heat content within melt also developed enormous solidification stress to facilitate crack formation [9, 10]. The presence of blow holes/pores and tiny cracks at subsurface acted as stress concentration zone and became the nucleation site for main crack formation during service.

With respect to the specification, nickel content was too low for the investigated alloy. Normally, Ni content of 4.5–7.0 wt.% becomes effective in suppressing pearlite transformation and promoting martensite transformation along with retained austenite. However, low Ni content (usually 0.2–1.5 wt.% and in present context  $\sim 0.5$  wt.%) in present context did not promote pearlite formation. The reason was Mo concentration to the tune of  $\sim 0.5$  wt.%, which restricted pearlite formation for large casting [11].

Excessively low Ni content reduced the toughness of the component, i.e., the alloy became brittle. Depending on section thickness, adequate Ni addition is necessary to control the formation and distribution of brittle carbide [12]. As Ni content was low, abrasion and fracture resistance of the present alloy were reduced drastically. Moreover, some amount of tungsten was found within the alloy composition. Normally uniform distribution of tungsten rich carbide improves hardness and resistance against wear [13]. At the same time, tungsten alters the nature of secondary carbides and turns the alloy brittle if clustering occurs. In the investigated microstructure, tungsten contributed in forming large complex carbides for the roller material. Therefore, the presence of tungsten reduced impact toughness of the alloy and encouraged brittle fracture [14]. Deviation in composition with respect to specification thus caused embrittlement to the investigated alloy.

The matrix of white cast iron consisted of martensite ( $\alpha'$ ) with small amount of retained austenite ( $\gamma$ -Fe, 15% by volume). Distribution of complex alloy carbides ( $M_7C_3$ ) was found within matrix. It was difficult to obtain fully

martensitic structure as the Cr content was < 12 wt.%. This type of eutectic carbide becomes major microstructural constituent for this grade of cast iron. Well dispersion and uniform size range of  $M_7C_3$  in general contribute to high hardness and adequate wear/abrasion resistance of the alloy. With respect to the same, the present investigation revealed the presence of substantial quantity of large size/inter-connected alloy carbides. Even in the presence of Mo such kind of morphology indicated inappropriate cooling rate [15]. This characteristic of second phase significantly reduced the ductility of the alloy.

High bulk hardness near fracture location of damaged component became at par with the microstructure of the alloy. The deviation in composition with morphological change in carbides raised the bulk hardness of the component. Another contribution came from high residual stress near surface/at subsurface of the component. Residual stress appeared due to elastic response of a material to an inhomogeneous distribution of non-elastic strains such as plastic strains, precipitation, phase transformation, and thermal expansion strains. The residual stress was tensile in nature. Apart from stress related to solidification, the contribution also came from deposition welding. As evident from composition difference, there was thermal mismatch between parent alloy and weld deposit. After deposition welding, difference in thermal contraction coefficient of two materials developed tensile residual stress. In present investigation, deposition direction corresponded to thickness direction. The quantification and determination of nature of residual stress have been done in all three directions. In comparison with other two, the value was significantly higher in the direction, which was perpendicular to the plane of the crack propagation. The tensile residual stress can significantly reduce the fatigue strength after deposition welding by decreasing the crack initiation period [16, 17]. The stress was further contributed to reducing the ductility of the alloy. The lowering in toughness was manifested by extremely low fracture toughness of the material.

The presence of ‘kidney’-shaped region and striations over fracture surface were the signature of cyclic loading over vertical roller during operation. This type of loading was related to the rotation of the component. At any instant, when the surface of vertical roller was in contact with liner table to crush raw materials, the load became maximum. Subsequently, the out of the contact position of roller periphery with respect to liner table corresponded to minimal load. Cyclic loading of such nature triggered crack formation from stress concentration sites like blow/pin holes and micro-cracks. During service, the crack propagated leaving behind the signature of striations endorsing the characteristic of fatigue. Similar type of characteristic is also illustrated in studies for various components with

limited ductility/composite structure [18–20]. The crack propagation was facilitated by the limited ductility, i.e., high hardness of the alloy. Moreover, the existence of large complex carbides and high residual stress also steered crack propagation through thickness direction. After traversing nearly 2/3 distance over the fracture plane, the load-bearing ability of the component was dropped drastically, and rest of the component failed through fast fracture.

The results and subsequent discussion showed that multiple reasons played influential role for the de-generation of vertical roller during service. These factors are highlighted below:

- The presence of blow/pin holes and tiny cracks at the subsurface level of vertical roller acted as stress concentration sites.
- Low nickel and substantial quantity of tungsten content in bulk composition of the failed component reduced ductility of the alloy drastically.
- The presence of bulky carbides diminished the toughness of the alloy considerably.
- Neither pre-heating nor post-weld heat treatment was adopted at the time of welding, which generated enormous residual stress within the component.

## Summary and Conclusions

Detail investigation has been carried out for the damaged vertical roller of grinding mill of cement plant. The observations are illustrated below:

- With respect to standard specification of similar type of alloy, the composition of damaged component exhibited significantly low nickel ( $\sim 0.5$  wt.%) and high tungsten ( $\sim 1.0$  wt.%) content.
- Dendritic microstructure of the alloy consisted of martensitic matrix and small amount of retained austenite. Alloy carbides were present as second phase in two different size ranges: One was small ( $< 50 \times 10 \mu\text{m}^2$ ), and the other one was extremely large ( $> > 50 \mu\text{m}$ ).
- The bulk hardness of the alloy ( $\sim 654$  BHN) adjacent to failed location was considerably higher than that of the white cast iron of equivalent/similar grade (550–600 BHN).
- The residual tensile stress below the subsurface of cracked plane of the component was high ( $\sim 170$  Mpa) and facilitated easy crack propagation during service.
- Fracture surface illustrated transgranular cleavage morphology, which became the signature of extremely low ductility.



- The subsurface region below cracked plane adjacent to open edge was decorated with blow/pin holes ( $\phi < 1.0$  mm) and fine cracks (length 0.2–2.0 mm). The location served as stress concentration site, where the fatigue crack was nucleated during cyclic loading. Fatigue crack moved fast due to low toughness of the alloy, the presence of chunky complex carbides, and high residual stress leaving behind the mark of striations. Under heavy grinding load, the crack reached at a critical length and the rest of the component failed due to fast fracture.

### Recommendation

- De-gassing of the melt and maintaining of specific alloy composition during casting are prerequisite to achieve desired composition and subsequently properties of the product.
- At the time of deposition welding, pre-heating of the region of interest may be attempted to minimize the temperature difference between arc and substrate.

**Acknowledgment** Authors are grateful to Director, CSIR-NML, for providing the infrastructural support to carry out the investigation and accord permission to publish the work.

### References

1. E. Amrina, M. Oktaviani, Potential failure modes of cement production process: a case study. Proceedings of the International Manufacturing Engineering Conference and the Asia Pacific Conference on Manufacturing Systems, Springer: Singapore pp 205–210, 2019
2. Grinding plate wear failure analysis, ASM failure analysis case histories: machine tools and manufacturing equipment. *SM Int.* <https://doi.org/10.31399/asm.fach.machtools.9781627082235> 2019
3. M.D.M. Neves, A.H.P. Andrade, D.N. Silva, Analysis of the criticality of flaws found in trunnion of grinding ball mills used in mining plants. *Engg. Failure Ana.* **61**, 28–36 (2016)
4. R.S. Sinha, A.K. Mukhopadhyay, Failure rate analysis of Jaw Crusher: a case study. *Sādhanā.* **44**(17), 1–9 (2019). <https://doi.org/10.1007/s12046-018-1026-4>
5. R. Eshghian, M. Abbasi, Wear and failure analysis of semi-autogenous grinding mill liners. *J. Failure Ana. Prevention.* **17**(2), 340–348 (2017). <https://doi.org/10.1007/s11668-017-0249-8>
6. S.S. Ngiam, F.P. Brennan, Fatigue crack control in structural details using surface peening. *J. Ship Prod.* **24**(3), 147–151 (2008)
7. C.R.S. Da Silva, M. Boccalini, Thermal cracking of multicomponent white cast iron. *Mats. Sci. Technol.* **21**(5), 565–573 (2005)
8. H. Mohebbi, D.A. Jesson, M.J. Mulheron, P.A. Smith, Characterisation of the fatigue properties of cast irons used in the water industry and the effect on pipe strength and performance. *J. Phys. Conf. Ser.* **181**, 012039 (2009). <https://doi.org/10.1088/1742-6596/181/1/012039>
9. H. Farhangi, S. Norouzi, M. Nili-Ahmadabadi, Effects of casting process variables on the residual stress in Ni-base super alloys. *J. Mats. Proc. Technol.* **153–154**, 209–212 (2004)
10. A.A. Keste, S.H. Gawande, C. Sarkar, Design optimization of precession casting for residual stress reduction. *J. Comp. Des. Eng.* **3**(2), 140–150 (2016)
11. X.R. Chen, Q.J. Zhai, H. Dong, B.H. Dai, H. Mohrbacher, Molybdenum alloying in cast iron and steel. *Adv. Manuf.* **8**, 3–14 (2020)
12. A.N. Sudhakar, R. Markandeya, R.B. Srinivasa, A.K. Pandey, D. Kaushik, Effect of alloying elements on the microstructure and mechanical properties of high chromium white cast iron and Ni-hard iron. *Mats. Today Proceed.* **61**(3), 1006–1014 (2022)
13. E. Cortes-Carrillo, A. Bedolla-Jacuinde, I. Mejia, C.M. Zepeda, J. Zuno-Silva, F.V. Guerra-Lopez, Effects of tungsten on microstructure and on the abrasive wear behaviour of a high chromium white cast iron. *Wear.* **376–377**, 77–85 (2017)
14. D. Myszka, J. Kasinska, A. Penkul, Influence of tungsten on the structure and properties of ductile iron containing 0.8% Cu. *Arch. Foundry Eng.* **21**(4), 121–126 (2021). <https://doi.org/10.24425/afe.2021.139760>
15. Z. Zhao, Y. Cao, X. Wan, J. Li, G. Li, Effect of cooling rate on carbide characteristics of high vanadium high speed steel. *ISIJ Int.* **62**(3), 524–531 (2022)
16. A.K. Syed, B. Ahmad, H. Guo, T. Machry, D. Eatock, J. Meyer, M.E. Fitzpatrick, X. Zhang, An experimental study of residual stress and direction-dependence of fatigue crack growth behaviour in as-built and stress relieved selective-laser-melted Ti6Al4V. *Mats. Sci. Engg. A.* **755**, 246–257 (2019)
17. A. Trudel, M. Brochu, M. Levesque, Residual stress effects on the propagation of fatigue crack in the weld of a CA6NM stainless steel, 13th International Conference on Fracture. Beijing, China 2013
18. A. Jameel, G.A. Harmain, Fatigue crack growth in presence of material discontinuities by EFGM. *Int. J. Fatigue.* **81**, 105–116 (2015)
19. Y. Liu, S. Liu, Optimization design of unbonded areas layout in Titanium alloy laminates for fatigue performance. *Symmetry.* **14**, 1836 (2022). <https://doi.org/10.3390/sym14091836>
20. R.O. Ritchie, Mechanisms of fatigue crack propagation in ductile and brittle solids. *Int. J. Fract.* **100**, 55–83 (1999)

**Publisher's Note** Springer Nature remains neutral with regard to jurisdictional claims in published maps and institutional affiliations.

Springer Nature or its licensor (e.g. a society or other partner) holds exclusive rights to this article under a publishing agreement with the author(s) or other rightsholder(s); author self-archiving of the accepted manuscript version of this article is solely governed by the terms of such publishing agreement and applicable law.